Theoretical study of the stabilization of cubic-phase ZrO_2 by impurities

E. V. Stefanovich and A. L. Shluger
The Royal Institution of Great Britain, 21 Albemarle Street, London W1X 4BS, United Kingdom
and Department of Chemical Physics of Condensed Matter, University of Latvia, 19 Rainis Boulevard, Riga, LV-1586 Latvia

C. R. A. Catlow
The Royal Institution of Great Britain, 21 Albemarle Street, London W1X 4BS, United Kingdom
(Received 13 December 1993)

We have performed a thermodynamical analysis of the phase diagrams for ZrO_2-CaO and ZrO_2-MgO solid solutions which has demonstrated that differential heats of mixing are important parameters determining the stabilization of the cubic phase of ZrO_2 by impurities. It is shown that the differential heats of mixing in the cubic phase of these systems should be lower than in the tetragonal phase. To understand this effect we have studied the electronic and geometrical structures of the pure and doped ZrO_2 crystals. Three computational techniques were employed: the *ab initio* Hartree-Fock pseudopotential method is used to study the atomic and electronic structures of the three phases of pure ZrO_2 crystals; the defect energies and the differential heats of mixing values are calculated by means of the atomistic simulation technique using the shell model and the pair-potential approximation; the self-consistent semiempirical intermediate neglect of differential overlap method is used to study changes in the electronic structure imposed by the defects. From the results of various calculations, we are able to identify the key factors contributing to the mechanism of stabilization of cubic ZrO_2 by impurities. These include the lattice distortion around vacancies, the lowering of the dielectric constant in the cubic phase, the impurity-stimulated increase of ionicity, and the removal of the Zr orbital degeneracy.

I. INTRODUCTION

Zirconia (ZrO_2) is an important technological material. It has broad applications in oxygen sensors, high-temperature fuel cells, as a refractory material in metallurgy, and as a thermal barrier coating in engines.[1] Zirconia has three low-pressure structural modifications which have different physical and thermomechanical properties. At low temperatures ZrO_2 has a monoclinic (m) structure (space group $P2_1/c$).[2] At temperatures of $T_{m\text{-}t} \approx 1400$ K the first-order displacive martensitic phase transition to the tetragonal (t) phase (space group $P4_2/nmc$) occurs.[1,3] At temperatures higher than $T_{t\text{-}c} = 2650$ K tetragonal ZrO_2 transforms into the cubic (c) fluorite lattice (space group $Fm3m$).[4] Both m and t structures can be considered as distorted cubic structures (see Fig. 1). Geometrically, the atomic structure of the t phase can be obtained from that of the c phase by a displacement of oxygen ions along the c axis as shown in Fig. 1, accompanied by a change of lattice parameters. This displacement, which drives the phase transition between the two phases, is referred to as the X_2^- mode. This notation corresponds to the symmetry analysis of phonon modes in the c phase performed in Ref. 5.

Addition of impurities like Ca^{2+}, Mg^{2+}, or Y^{3+} improves substantially the thermomechanical properties of ZrO_2, allowing the production of materials with extremely high strength, toughness, and thermal-shock resistance.[1] It is known that these properties are closely related to the stabilizing effect of impurities on the cubic phase. The stabilization is manifested by the lowering of the temperature of the cubic solid-solution field in the experimental phase diagram (see Fig. 2). Similar stabilization of the t phase with respect to the m phase also occurs.

In spite of extensive experimental studies there is no clear understanding of the role played by impurities in the cubic-phase stabilization. Several factors which can influence the stabilization have been proposed, but no detailed mechanism has been developed thus far.

Dwivedi and Cormack[6] suggested that the cubic phase is stabilized by doping with cations such as Ca^{2+} due to the larger size of the Ca^{2+} ion, which imposes a local cubic symmetry on the anion sublattice. Cormack and Parker[7] calculated the phonon spectra of pure and doped c-ZrO_2 crystals. They obtained an imaginary frequency for the X_2^- mode in the pure crystal and concluded that the c phase does not correspond to a local minimum of the adiabatic free-energy surface (AFES). On adding the impurity they calculated that the frequency of this mode becomes positive, which was interpreted as a creation of a local minimum of the AFES corresponding to the c phase. This was identified with the "stabilization" of the c phase by dopants. Indeed these calculations clearly reveal an important effect of dopants on the lattice dynamics and hence the free energy of the solid. However, the existence of the total-energy minimum does not necessarily imply that the c phase has a lower free energy than the t phase, and, therefore, does not prove its relative thermodynamic stability.

In this work we use a more general approach to the study of the relative stability of different phases, which is based on a comparison of their free energies as a function of dopant concentration and temperature. First, we per-

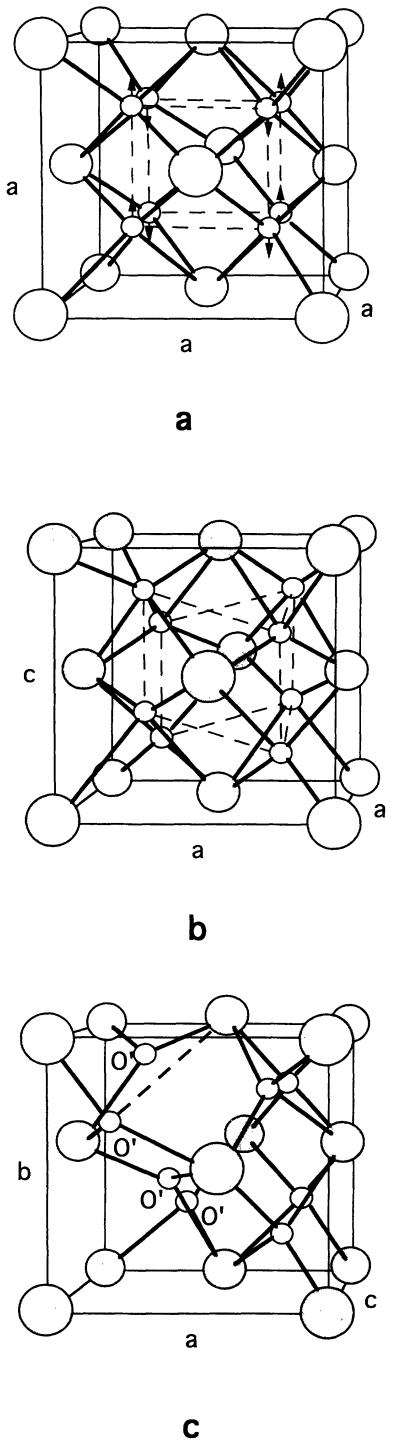

FIG. 1. Schematics of the three ZrO_2 polymorph structures. Small circles represent the oxygen atoms; large shaded circles represent the zirconium atoms. a, b, and c indicate the crystalline axes. (a) c-ZrO_2. The arrows show the directions of displacements of the oxygen atoms corresponding to the X_2^- distortion which transforms the c structure into the t structure. (b) t-ZrO_2. Note the deformation of the oxygen sublattice (dashed lines) with respect to that in the c structure. (c) m-ZrO_2. In contrast to the t and c structures Zr atoms are seven coordinated and O' atoms are three coordinated: the Zr-O' bond which is shown by a dashed line is broken. Note that the unit cell is rotated with respect to that in (b).

form a simple phenomenological analysis of the low-concentration high-temperature parts of the experimental ZrO_2-CaO and ZrO_2-MgO phase diagrams, which demonstrates that the differential heats of mixing (DHM's) of impurities in different phases are the key qualitative parameters which determine the t-c phase separation boundaries in the corresponding phase diagrams. Moreover, the differential heats of mixing F_0 for the cubic phase are found to be lower than those for the tetragonal phase. To understand the latter fact at a microscopic level, the values of F_0 for Ca and Mg impurities are calculated. For this purpose the atomic and electronic structure of the three phases of ZrO_2, MgO, and CaO perfect crystals are studied first. Then, in accordance with the existing models, two possible structures of $Zr_{0.875}Ca_{0.125}O_{1.875}$ and $Zr_{0.875}Mg_{0.125}O_{1.875}$ solid solutions are considered which correspond to the nearest-neighbor (NN) and next-nearest-neighbor (NNN) arrangements of the impurity ions and compensating oxygen vacancies. We show that the inequality $F_0^c < F_0^t$ between the DHM's for the c and t phases holds for these representative defect configurations. We are able to iden-

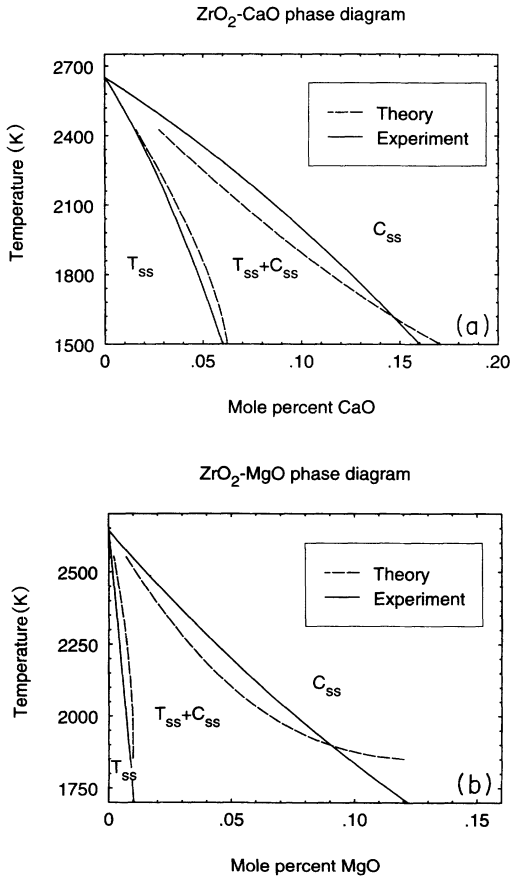

FIG. 2. Phase diagrams of concentration of impurities vs temperature. Full lines represent the experimental data, while dashed lines are the results of calculations using the expressions (1) and (2) for the free energy of the solid solution, Eq. (3) for the solubility lines, and the fitted DHM values from Table I. (a) ZrO_2-CaO system, experimental data from Ref. 14; (b) ZrO_2-MgO system, experimental data from Ref. 15.

tify several factors at the microscopic level, which can cause the lowering of the t-c phase transition temperature in the presence of the Ca and Mg dopants.

The calculation techniques used in the present study are based on the supercell model for pure and defective crystals. The *ab initio* Hartree-Fock pseudopotential method[8] (the CRYSTAL code[9]) is employed to study the atomic and electronic structures of the three phases of pure ZrO_2 crystals. The defect energies and the DHM values are calculated by means of the atomistic simulation technique (the GULP code[10]) using the shell model and the pair-potential approximation. The self-consistent semiempirical intermediate neglect of differential overlap (INDO) method and the CLUSTER computer code[11,12] are used to study changes in the electronic structure imposed by the defects.

A brief outline of the calculation techniques is given in Sec. III; comparison of the properties of the three phases of zirconia calculated by different methods is presented in Sec. IV A. Detailed comparison of the CLUSTER and GULP calculated defect properties is given in Sec. IV B. Several possible mechanisms of the stabilization of the cubic phase by impurities are proposed and discussed in Sec. V.

II. THERMODYNAMIC ASSESSMENT OF THE EXPERIMENTAL PHASE DIAGRAMS

The thermodynamic analysis of the phase diagrams[13] is the most direct way to find out the key parameters which determine the relative stability of different phases. In this section we aim to fit the experimental phase diagrams (see Refs. 14 and 15 and references therein) using the general procedure described in Ref. 13 and the simplest possible phenomenological expression for the free energy as a function of impurity concentration x and temperature.

Different expressions for the free energy have been used to fit the experimental data with high accuracy for all values of T and x in $(ZrO_2)_{1-x}$-$(CaO)_x$ and $(ZrO_2)_{1-x}$-$(MgO)_x$ systems.[14,15] We are interested in a restricted region of the phase diagram which is important for the study of the mechanism of stabilization of the cubic phase [small concentrations ($x<0.25$) and high temperatures ($T>1500$ K)]. We have used the following general expression for the free energy of the ZrO_2-CaO solid solution per mole of cation:[13,16]

$$F^i(x,T)=(1-x)F^i_{ZrO_2}(T)+xF_{CaO}(T)+F_{ideal}(x,T)+F^i_{ex}(x,T) . \quad (1)$$

A similar expression is valid for the ZrO_2-MgO solid solution. The index $i(=m,t,c)$ corresponds to the three polymorphs of zirconia. The standard representation[17] was taken for the free energies of the pure oxides $F_{CaO}(T)$ and $F_{MgO}(T)$. For the free energy of pure t- and c-ZrO_2 the experimental data from Ref. 18 were fitted as follows:

$$F^t_{ZrO_2}(T)=-92\,167-54.57(T-2650)+H^0_{298}\ (\text{cal/mol}) ,$$

$$F^c_{ZrO_2}(T)=-92\,167-55.07(T-2650)+H^0_{298}\ (\text{cal/mol}) ,$$

where H^0_{298} is the enthalpy of formation in the standard state. $F_{ideal}(x,T)$ represents the "ideal" part of the free energy of mixing.[16] If we assume that the number of impurity ions is equal to that of the compensating vacancies (see next section), the term $F_{ideal}(x,T)$ can be easily calculated from the number of permutations of the n Ca (Mg) ions and n oxygen vacancies over the available N zirconium and $2N$ oxygen sites ($n/N=x$):

$$F_{ideal}(x,T)=RT[x\ln(x)+(1-x)\ln(1-x)+(2-x)\ln(1-x/2)+x\ln(x/2)] .$$

In the simplest *zeroth approximation* of the molecular theory of solutions[16] the excess free energy of solution $F^i_{ex}(x,T)$ does not depend on temperature, and its concentration dependence may be expressed as

$$F^i_{ex}(x)=F^i_0x(1-x) . \quad (2)$$

Here F^i_0 are the differential heats of mixing which should be fitted to reproduce the experimental phase diagram.

The tetragonal and cubic solubility lines [$x_t(T)$ and $x_c(T)$ respectively] determine the boundaries of the t-c two-phase region, where both t and c solid solutions coexist. The solubility lines satisfy the following set of nonlinear equations:

$$F^t(x_t(T),T)+F'^t(x_t(T),T)[x_c(T)-x_t(T)]=F^c(x_c(T),T) , \quad (3)$$

$$F'^t(x_t(T),T)=F'^c(x_c(T),T) ,$$

where primes denote derivatives over x. Solving these equations, the F^t_0 and F^c_0 were optimized to achieve the best fit of the experimental $x_t(T)$ and $x_c(T)$ functions.[14,15] Note that the observed stabilization of the cubic phase requires that the DHM for the cubic phase must be lower than that for the tetragonal phase:

$$F^c_0<F^t_0 . \quad (4)$$

The values of the fitted parameters presented in Table I show the validity of this qualitative conclusion. The calculated c, $t+c$, and t phase fields are presented in Fig. 2,

TABLE I. The differential heats of mixing (eV) of Ca-vacancy and Mg-vacancy dipoles. Fitted values were obtained by fitting the $t-t+c$ and $t+c-c$ phase boundaries on the x-T phase diagram as described in Sec. II.

	F^m_0	F^t_0	F^c_0
Ca GULP NNN	1.00	0.36	0.26
Ca GULP NN	1.02	0.06	−0.10
Ca fitted		0.50	0.27
Mg GULP NNN	2.50	1.55	1.39
Mg GULP NN	2.66	1.73	1.56
Mg fitted		1.89	1.38

where they are compared with the experimental data.[14,15]

These results clearly demonstrate that the experimental phase diagrams can be qualitatively reproduced in the simple approximation (1) and (2) with a minimal number of fitting parameters. The DHM's which determine the qualitative behavior of the solubility lines do obey the inequality (4). In the following sections we present the results of atomistic calculations which address the question of the reasons why the DHM for the cubic phase is lower than that for the tetragonal phase. In this way we hope to gain a better understanding of the micromechanisms of stabilization of the cubic phase.

III. CALCULATION TECHNIQUES

The calculation techniques used in this study (*ab initio* Hartree-Fock, semiempirical Hartree-Fock, and atomistic simulation) are based on the periodic supercell model for both perfect and doped crystals. This allows us to optimize not only local structure but also unit-cell parameters for each crystalline phase, defect type, and concentration.

A. *Ab initio* Hartree-Fock method (CRYSTAL code)

The *ab initio* calculations were performed using the periodic Hartree-Fock linear combination of atomic orbitals (LCAO) method described in detail in Refs. 8 and 9. Effective core potentials (ECP's) were used for oxygen and zirconium. The so-called small-core version of the Hay-Wadt ECP[19] was employed for the Zr atoms. This pseudopotential corresponds to 12 explicitly treated valence electrons. The ECP from Ref. 20 was used to represent the cores of the oxygen atoms. The detailed description of the method and the Gaussian basis set will be published elsewhere.[21] In what follows we shall refer to this technique as the CRYSTAL method.

B. Semiempirical INDO method (CLUSTER code)

The modification of a self-consistent semiempirical Hartree-Fock method employed in this work has been described elsewhere[11,12] and realized in the CLUSTER computer code. We use the periodic large unit cell (LUC) model[22] and the INDO approximation of the restricted Hartree-Fock-Roothaan method.[23] It allows us to determine the electronic structure of a quantum-mechanically described periodic cell that contains several tens of ions. It employs a minimal valence Slater basis set and uses a single-determinantal approximation for the wave function.

The study of the structural modifications of the ZrO_2 crystal and defects therein requires definition of the one- and two-center parameters describing Zr, O, Mg, and Ca ions and their interaction. In this study we used the parameters for the O and Mg ions from Ref. 12, and those for the Ca ions from Ref. 24. They are summarized in Tables II and III. The parameters for the Zr ions were obtained in this work following the general procedure described in Ref. 12. In optimizing their values the results of the *ab initio* calculations for the ZrO (Ref. 25) and ZrO_2 molecules, as well as those for the *t* and *c* phases of ZrO_2 crystal, were taken into account.

The ZrO_2 molecule was computed in this work using the Möller-Plesset perturbation (MP2) method and the CAD-PAC5 computer code[26] with the MPP pseudopotential for Zr atoms developed in Ref. 27. The standard 6-311G* basis set on oxygen atoms[28] and the valence 311G basis set on Zr atoms[27] were used in these calculations. The bent conformation of the molecule (C_{2v} symmetry, $d_{Zr\text{-}O}=3.45$ bohr, $\angle$O-Zr-O$=109.5°$) was found to be more stable than the linear conformation by about 2.7 eV. Good agreement between the *ab initio* data and CLUSTER results was achieved for the equilibrium geometry and the electronic charge distribution in the ZrO and ZrO_2 molecules.

The calculated atomization energies and the characteristic parameters of the electronic structure of the perfect crystals, such as valence bandwidths and band gaps (computed at optimized geometries) are presented in Table IV. The lattice constants calculated for the CaO and MgO crystals (4.79 and 4.07 Å, respectively) are in good agreement with the experimental data. The unit-cell parameters for the three structural modifications of ZrO_2 are presented in Table V.

It is well known that the one-electron band gaps found in the Hartree-Fock band-structure calculations considerably overestimate the experimental values.[36] The so-called long-range correlation corrections are usually used for more correct comparisons of the theoretical and experimental gap values. The correlation corrections for the CaO and MgO crystals were calculated to be 3.25 and 5.21 eV, respectively.[32] The corresponding values for the ZrO_2 polymorphs have not been calculated thus far. In this paper we used the same correction for all three polymorphs of ZrO_2. It was estimated by averaging the existing data for other ionic crystals[37] as 3.8 eV.

MgO and CaO crystals are highly ionic; the effective charges of the oxygen ions were computed to be $-1.84|e|$ and $-1.87|e|$, respectively. The orbital populations for the three ZrO_2 polymorphs are discussed in Sec. IV.

TABLE II. One-center INDO parameters. The conventional definition of the parameters is used, as described in Refs. 12 and 23.

	O	Zr	Ca	Mg
ζ (spd) (a.u.$^{-1}$)	2.27; 1.86	1.90; 1.90; 1.83	1.48	1.40
Eneg (spd) (eV)	4.5; −12.6	8.0; −8.0; 4.6	12.0	16.0
$-\beta$ (spd) (eV)	16.0; 16.0	0.5; 0.5; 11.0	0.4	1.1
P_0 (spd) (a.u.)	1.974; 1.96	1.0; 0.0; 0.6	0.15	0.15

TABLE III. Two-center INDO parameters for the interactions between electrons (A) and cores (B) (a.u.$^{-1}$). See Ref. 12 for more details. n.o. means that the parameter was not optimized.

A	B: O	Mg	Ca	Zr
O	0.15	0.25	0.17	0.0
Mg	0.0	0.25	n.o.	0.0
Ca	0.1	n.o.	0.15	0.0
Zr	0.0	0.0	0.0	0.0

C. Atomistic simulation technique (GULP code)

The binding of ionic solids may be simplistically described by the Born model in which formally charged ions interact via electrostatic forces (evaluated by the method of Ewald to ensure rapid convergence) supplemented by a short-range Buckingham potential

$$E_{ij} = A_{ij}\exp(-r_{ij}/\rho_{ij}) - C_{ij}/r_{ij}^6 .$$

These short-range parameters may be determined empirically by fitting to crystal properties or derived from quantum-chemical energy surfaces obtained by electron-gas *ab initio* methods. The model is refined by inclusion of dipole polarizability through the shell model.[38]

The shell-model parameters for oxygen ions and the parameters of O-O, Ca-O, and Mg-O pair potentials employed in this study were taken from Ref. 39. The parameters for Zr-Zr and Zr-O interactions were fitted in Ref. 6. The latter parameters allow us to reproduce qualitatively correctly the relative energetic stability of all three phases of ZrO_2 (see Table V), and their dielectric and elastic constants in good agreement with experiment.[6] Therefore, these potentials seem adequate at least for a qualitative study of properties of pure and doped ZrO_2 in different polymorphs.

The major part of the defect calculations using the GULP code and all the CLUSTER calculations were performed using the same supercell containing 24 atoms which is a $2\times2\times2$ extension of the unit cell of cubic ZrO_2. This allows us to compare directly results obtained by the two techniques. Placing one dopant ion (and one oxygen vacancy) in each supercell, we obtain an impurity concentration of 12.5% which is characteristic for cubic partially stabilized ZrO_2.

IV. RESULTS OF CALCULATIONS

A. Perfect crystal

1. Definition of different phases

It is currently believed that both the m-t and t-c phase transitions in ZrO_2 are first order.[18] (Note, however, that the experimental results for the t-c transition are quite uncertain and one cannot exclude the possibility of a second-order t-c transition[40].) Theoretically, a system which undergoes a first-order transition can be described in terms of the AFES,[40,41] where both low- and high-symmetry structures correspond to different local minima. The low-symmetry phase has higher vibrational frequencies and thus a lower vibrational entropy, which results in its instability at temperatures higher than the transition point.[42] A system which undergoes a second-order transition can be described in terms of the double-well structure of the AFES, when both wells converge to one high-symmetry minimum at temperatures higher than the critical point.

Some valuable information regarding the main features of the AFES (location of minima and saddle points between them, relative energies of different phases, phonon frequencies, etc.) may be obtained from calculations at zero temperature. In this case, the AFES coincides with the adiabatic energy surface (AES) (apart from the zero-point energy correction). Using results of the AES calculations one can extrapolate the behavior of the AFES to nonzero temperatures and speculate regarding the nature of the phase transition.[42] For instance, the temperature of the second-order transition can be estimated from the height of the barrier separating two low-symmetry minima of the AES if one takes into account the thermal ex-

TABLE IV. The atomization energies per one formula unit, the electronic energy gaps, and the widths of the valence bands of crystals (eV) computed using the CLUSTER code. The experimental data and the results of *ab initio* calculations are given in parentheses.

Crystal	Atomization energy	Energy gap	Valence bandwidth
m-ZrO_2	15.2 (15.7[a]; 22.7[b])	5.25 (4.70[c]; 4.51[d])	10.5 (4.97[d])
t-ZrO_2	14.9 (15.7[a])	3.05 (4.11[d])	13.2 (7.14[a]; 5.48[d])
c-ZrO_2	14.9 (15.5[a])	2.88 (3.84[d])	13.6 (7.97[a]; 5.90[d])
CaO	8.1 (10.3[b])	7.34 (7.73[e]; 7.09[f])	3.0 (3.43[e])
MgO	8.1 (11.0[b])	6.53 (8.21[e]; 7.83[f])	5.7 (7.64[e]; 6.7[g])

[a]Reference 29.
[b]Calculated from data in Ref. 17.
[c]Reference 30.
[d]Reference 31.
[e]Reference 32.
[f]Reference 33.
[g]Reference 34.

pansion of the crystal as suggested in Ref. 35.

In our calculations we adopted the following definitions for the m, t, and c structures of the perfect and doped crystals. The geometry of the m structure (comprising the unit-cell dimensions and fractional coordinates of atoms) was optimized subject to the condition $\alpha=\beta=90°$. The t structure corresponds to the following restrictions imposed on the lattice parameters: $a=b$; $\alpha=\beta=\gamma=90°$. The most severe restrictions on the unit-cell dimensions were imposed for the c structure: $a=b=c$; $\alpha=\beta=\gamma=90°$. This representation of the stabilized c structure is consistent with diffuse-neutron-scattering experiments.[43,44] Note, however, that other models have also been suggested in the literature. In particular, Martin, Boysen, and Frey[45] proposed that the cubic solid solution may consist of t-phase microdomains, whereas Rossell, Sellar, and Wilson[46] suggested that it is constructed from ϕ_1-phase microdomains.

Little is known about the form of the AES of the ZrO_2 crystal. In particular, it is not clear whether the t and c phases correspond to a local minimum of the AES or whether they are unstable saddle-point configurations.[7,29,35,47] Although it is clear that the energies of the three structures (at 0 K) should be related as

$$E^m<E^t<E^c ,$$

the numerical values of the energy differences have not yet been computed accurately. In the next subsection we present the results of our calculations of the AES of the ZrO_2 crystal using the CRYSTAL, CLUSTER, and GULP techniques.

2. The results of the AES calculations

The results of geometry optimization of the three crystalline modifications of ZrO_2 (the unit-cell parameters and fractional coordinates) using the calculation techniques described above are reported in Table V. The experimental structures and the results of recent full-potential linearized augmented-plane-wave (FLAPW) calculations[35] are also included for comparison.

The CRYSTAL calculations give the double-well structure of the AES for t-ZrO_2 with respect to the X_2^- displacement of the oxygen ions (see also Refs. 29 and 47). Both the difference between the t and c energies and the X_2^- shift of the oxygen ions (see Fig. 1) in the t structure

TABLE V. 0-K equilibrium geometries for the three phases of ZrO_2. The cell parameters a, b, c in Å. In m-ZrO_2, γ is in degrees and x_i, y_i, z_i denote the fractional coordinates of the ith symmetry-independent species. In t-ZrO_2, d_z is the displacement of oxygen along the X_2^- mode with respect to the ideal cubic position, in units of c. Energies are in eV per one formula unit of ZrO_2. Deviations from experimental values (as a percentage) are given as subscripts.

	CRYSTAL (this work)	CLUSTER (this work)	GULP (this work[a])	FLAPW (Ref. 35)	Expt. (Refs. 2, 4)
			m-ZrO_2		
a	$5.234_{1.6}$	$5.145_{-0.1}$	$5.241_{1.7}$		5.151
b	$5.272_{1.2}$	$5.178_{-0.7}$	$4.898_{-6.0}$		5.212
c	$5.398_{1.5}$	$5.003_{-5.9}$	$5.578_{4.9}$		5.317
γ	$98.25_{-1.0}$	$102.37_{3.2}$	$90.0_{-9.3}$		99.23
x_{Zr}	$0.2725_{-1.1}$	$0.2743_{-0.4}$	$0.2500_{-9.2}$		0.2754
y_{Zr}	$0.0343_{-13.2}$	$0.0276_{-30.1}$	$0.0000_{-100.}$		0.0395
z_{Zr}	$0.2098_{0.7}$	$0.2126_{2.1}$	$0.1899_{-8.8}$		0.2083
$x_{O(1)}$	$0.0723_{3.3}$	$0.0962_{37.4}$	$0.0753_{7.6}$		0.0700
$y_{O(1)}$	$0.3318_{0.0}$	$0.3717_{12.1}$	$0.2818_{-15.0}$		0.3317
$z_{O(1)}$	$0.3497_{1.5}$	$0.2930_{-15.0}$	$0.3958_{14.8}$		0.3447
$x_{O(2)}$	$0.4549_{1.2}$	$0.4584_{1.2}$	$0.4247_{-5.5}$		0.4496
$y_{O(2)}$	$0.7579_{0.1}$	$0.7456_{-1.5}$	$0.7182_{-5.1}$		0.7569
$z_{O(2)}$	$0.4802_{0.2}$	$0.4864_{1.5}$	$0.3958_{-17.4}$		0.4792
E^m-E^c	0.005	−0.299	−0.185		−0.120[b]
			t-ZrO_2		
$a=b$	$5.152_{2.0}$	$4.951_{-2.0}$	$5.074_{0.5}$	$5.049_{0.0}$	5.050[c]
c	$5.178_{-0.1}$	$4.961_{-4.3}$	$5.216_{0.7}$	$5.087_{-1.8}$	5.182[c]
d_z	$0.0246_{-57.1}$	$0.015_{-73.9}$	$0.060_{4.5}$	$0.029_{-49.5}$	0.0574[d]
E^t-E^c	−0.008	−0.008	−0.019	−0.008	−0.057[b]
			c-ZrO_2		
$a=b=c$	$5.154_{1.3}$	$4.940_{-2.9}$	$5.075_{-0.3}$	$5.054_{-0.7}$	5.090[c]

[a]See also Ref. 6.

[b]Enthalpy difference at the phase transition temperature (Ref. 18). Note that these values are in good agreement with the thermal energies estimated from the phase transition temperatures as $E^t-E^c=k(T_{t\text{-}c}-T_{m\text{-}t})/2=-0.112$ eV and $E^m-E^c=kT_{t\text{-}c}/2=-0.052$ eV.

[c]Extrapolation to zero temperature using the thermal expansion data from Ref. 4.

[d]At 1568 K.

are less than the experimental values. From these calculations it is not clear whether the tetragonal and monoclinic structures are separated by an energy barrier. More definite conclusions can be made after performing a more complete study of the AES. The detailed results of the *ab initio* CRYSTAL calculations of the three phases of ZrO_2 will be presented elsewhere.[21] We should note that Zhou and Jansen[48] have found local minima for both m and t structures using atom-atom potentials fitted to the results of their FLAPW calculations.

The CLUSTER and GULP techniques reproduce qualitatively the main geometrical parameters of the three phases. However, the most stable GULP geometry is more symmetrical (eight symmetry operations) than the real monoclinic structure (four symmetry operations) and corresponds to an orthorhombic space group. Both methods reproduce less accurately the positions of the O′ oxygen atoms (see Fig. 1) in m-ZrO_2. These atoms have the largest displacements in the course of the t-m phase transition: one of the Zr-O′ bonds is broken in the m structure, so that Zr atoms change their coordination number from 8 to 7. It is worth noting the close agreement between the geometrical parameters, dielectric, and elastic constants of the t and c phases obtained in this work by the GULP code and by Dwivedi and Cormack[6] using periodic boundary calculations employing the CASCADE code.[49] We consider this as an indicator of the accuracy of the GULP program.

Since the GULP method predicts instability of t and c phases at zero temperature, their phonon spectra contain imaginary frequencies. Therefore it is impossible to calculate their thermodynamical properties (entropy, free energy, thermal expansion coefficient, etc.). Note, however, that the instability of both phases at zero temperature corresponds to experimental observations. Since these phases are stable at high temperatures, one can approximately calculate the DHM values for the doped crystals by imposing constraints on the unit-cell shape and dimensions as described above. As was demonstrated, the DHM values are sufficient for a qualitative description of the free energies of the doped crystals given by Eqs. (1) and (2) and construction of the phase diagram.

Finally we should note that the energy difference $E^c - E^t$ is underestimated by all three calculation techniques used in this study (see Table IV). The agreement with the experimental data can be improved by taking into account the thermal expansion of the crystal as discussed in Ref. 35. For this purpose one can use the experimentally measured thermal expansion coefficients.[4]

B. Doped crystals

A full theoretical explanation of the c-phase stabilization requires calculation of the DHM values for different crystalline modifications, or, more exactly, the excess free energies of mixing. Generally speaking, the DHM values must satisfy the inequality (4). However, an accurate microscopic calculation of the DHM's is a complex problem. In order to obtain a qualitative understanding of the main factors which determine the micromechanism of stabilization of the c phase we will use simplified models and various approximations discussed below.

(i) We shall remain within the *zeroth approximation* of the molecular theory of solutions which was already used in Eq. (2). Assuming the validity of Eq. (2), we can express the DHM through zero-temperature lattice energies (a similar formula is valid for the ZrO_2-MgO solid solution):

$$F_0^i = \frac{E^i_{J(x)} - xE_{CaO} - (1-x)E^i_{ZrO_2}}{x(1-x)}, \tag{5}$$

where $J(x)$ is the most statistically abundant configuration(s) of defects. Generally speaking, in order to find the DHM values one should average expression (5) over all possible defect configurations according to their energies and (vibrational and configurational) entropies. The energies of various impurity-related defects and their aggregates were calculated by means of the atomistic simulation technique in Refs. 6, 50, and 51. However, no attempts have been made to our knowledge to use these data to calculate the partition function for the solid solution.

In the simplest approximation one or several representative configurations $J(x)$ can be chosen which correspond to the minimum of the crystal free energy at given concentration of impurities x. The lattice energies of the pure substances E_{CaO} (E_{MgO}) and $E^i_{ZrO_2}$ can be easily calculated within the Born model as discussed above. However, in order to calculate the $E^i_{J(x)}$ one needs to find the configuration $J(x)$. This point requires more detailed discussion.

(ii) It is known that the excess charge of divalent impurities in zirconia is compensated by the oxygen vacancies. Note that at $x \geq 0.1$ and high temperatures the impurity-vacancy dipoles are very closely located and the anion vacancies are mobile. Therefore it is difficult to distinguish between the different modes of compensation. For instance, the vacancies can occupy both the nearest-neighbor and the next-nearest-neighbor sites with respect to the impurity ion.[46] Both substitutional cation impurities and oxygen vacancies can be considered as nearly randomly distributed among available lattice sites.

However, in several works attempts have been made to specify the model in terms of a "preferable" location (NN[44,52,53] or NNN[6,46,54]) of the compensating vacancy and a relative distribution of the impurity-vacancy dipoles. In particular, in order to give an interpretation to the diffuse-neutron-scattering data, Neder, Frey, and Schulz[44] have studied the relative orientation of the neighboring NN Ca-vacancy dipoles. They have found that the best representation of the experimental results can be achieved if one assumes that adjacent dipoles have parallel or nearly parallel orientation. However, the suggested interpretations of these and other experiments[6,46,52,53,54] are model dependent and inconclusive.

Two simplified models of the ZrO_2-CaO and ZrO_2-MgO solid solutions were therefore studied in the present work. In both models we assumed that 1/8 of the Zr

atoms are substituted by impurities ($x=0.125$) distributed periodically in the lattice and forming the $2\times2\times2$ supercell. In the first model the compensating vacancies occupy the NNN positions, while in the second model the vacancies and impurity ions form the NN dipoles. In both models the dipoles in the adjacent supercells have parallel orientations. As will be shown below, the main conclusions drawn from the calculations on these two models are very similar. Therefore we believe that the most important factors relevant to the mechanisms of the cubic-phase stabilization can be identified already in this simplified approach.

Ca-vacancy NN dipole and Ca(Mg)-vacancy NNN dipole

The Ca-vacancy NN dipoles in ZrO_2 have been studied in several papers.[43,44,55,56] However, the results for defect relaxation and electronic structure differ significantly for the different techniques. For instance, the results of Ref. 55 predict that the introduction of the Ca-vacancy dipole increases the band gap of ZrO_2. The impurity-induced one-electron levels are found to be located high in the conduction band. It was concluded that the Ca ion interacts with the surrounding lattice mainly via electrostatic forces. These results contradict those of Ellis and co-workers[56] who found that the band gap is reduced substantially with respect to the pure crystal, and the Ca impurity levels are located near the top of the valence band. No calculations have been done thus far to our knowledge on the electronic structure of the impurity-vacancy NNN dipoles.

The complete optimization of the ionic coordinates around the NN and NNN Ca (Mg)-vacancy dipoles in the c structure was performed using only the GULP technique. To study the qualitative changes of the crystal electronic structure imposed by the defects we used the CLUSTER technique. The calculations were first performed using the ionic coordinates derived from the GULP calculations. Then an additional geometry optimization was made along the same relaxation modes (see, for example, modes 1–7 for the NNN dipoles in Table VI and Fig. 3). The lattice parameter a_0 was also optimized using both methods (see Table VII). It increases (decreases) when the Ca (Mg) impurities are introduced, in qualitative agreement with the experimental observations.[57,58]

In Table VI we compare the defect relaxations computed for the NNN dipoles by means of the GULP and CLUSTER methods. It can be seen that some of the displacements obtained by the two methods differ significantly. The reason is twofold. First, the CLUSTER relaxation is not complete since only a limited number of relaxation modes was included. Secondly, both methods use empirical parameters which were optimized for ideal crystals and may not be accurate for the representation of complex defect structures. Moreover, some of the ionic coordinates determined using both techniques for the pure m structure also differ substantially (see Table V). However, we found no significant difference in the electronic structure between the GULP defect geometry and that further optimized using the CLUSTER technique.

Some parameters of the electronic structure of the Ca (Mg) dipoles calculated using the CLUSTER method are presented in Table VII. The impurity-related, one-electron orbitals (orbital energy $\epsilon_{Ca(Mg)}$) are located high in the conduction band. The band-gap width E_g increases in the presence of Ca (Mg) impurities and there is a negligible admixture of the impurity orbitals with the mixed O(p)-Zr(d) valence band. These conclusions are in qualitative accord with the results of Ref. 55. Since an increase of the impurity concentration means substitution of the Zr ions with more electropositive Ca (Mg) ions, one can expect that the average ionicity of the crystal may also increase. The average electron population on the cations q_c and especially the d-shell population q_d (since the d orbitals of Zr form covalent hybrids with the p orbitals of oxygen atoms[29,31]) are suitable parameters for describing the degree of ionicity (covalency). The results presented in Table VII show that the ionicity indeed increases in the case of the Ca impurity (the average electron populations on cations and on their d orbitals decrease). This effect is less pronounced in the case of the Mg impurity.

The calculated DHM values for the three ZrO_2 polymorphs with full geometry optimization by the GULP method are presented in Table. I. As can be seen, the expected behavior $F_0^m > F_0^t > F_0^c$ is reproduced correctly for both NN and NNN dipole configurations.

TABLE VI. Comparison of the GULP and INDO geometries of the relaxed Ca-vacancy and Mg-vacancy NNN dipoles. Numbers of modes and directions of displacements along these modes are the same as in Fig. 3. The mode 1 corresponds to the shift of three Zr ions (not shown in Fig. 3) located in the positive direction of the threefold axis ⟨111⟩ with respect to the impurity ion.

		Displacements (Å)			
	Direction	Ca-vacancy		Mg-vacancy	
No. of mode	of displacements	GULP	CLUSTER	GULP	CLUSTER
1 (Zr)	away from Ca (Mg)	0.17	0.12	0.15	0.14
2 (O)	away from Ca (Mg)	0.30	0.71	0.29	0.80
3 (O)	away from Ca (Mg)	0.12	−0.14	0.05	−0.25
4 (Ca or Mg)	⟨111⟩	0.07	0.22	0.09	0.12
5 (O)	toward vacancy	0.45	0.29	0.43	0.26
6 (O)	toward vacancy	0.38	0.23	0.38	0.21
7 (O)	away from Ca (Mg)	0.25	0.09	0.20	−0.08

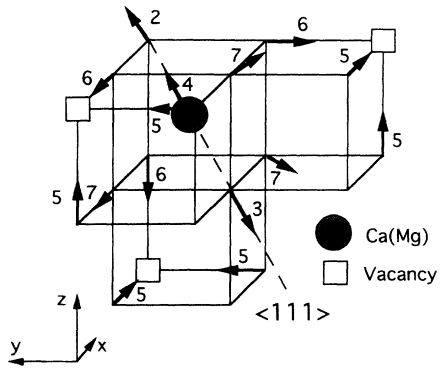

FIG. 3. Schematic of the NNN Ca (Mg) -vacancy dipole in c-ZrO_2. There are no separate dipoles in the lattice. Each impurity cation is surrounded by three oxygen vacancies symmetrically with respect to the threefold ⟨111⟩ axis. Arrows show the directions of ionic displacements obtained in the GULP calculations. The numbers by the arrows correspond to the relaxation modes in Table VI.

V. DISCUSSION

Let us consider the physical reasons which cause the perturbation created by the defects to be smaller in the high-symmetry phases than in the low-symmetry phases [see Eq. (4)]. This may be a result of several effects, some of which are discussed below.

(a) Vacancies. As was found by Dwivedi and Cormack,[6] the defect energy of a vacancy (and the corresponding contribution to the DHM) is lower in c-ZrO_2 than that in t-ZrO_2. Therefore the presence of vacancies makes the c phase more stable. The symmetrical relaxation of the nearest oxygen atoms around the vacant site (see Table VI and Fig. 3) imposes isotropic negative pressure on the anionic sublattice, which favors formation of an isotropic cubiclike structure around the vacancy and increases the energy of the anisotropic t structure. The importance of the oxygen vacancies for the c-phase stabilization was emphasized also in Refs. 40 and 59.

(b) Defect-defect interactions. The structure of the solid solution may be simplistically considered as a three-dimensional lattice (in general nonperiodic) consisting of charged "particles" (impurity ions and vacancies, $q \approx \pm 2.0$) embedded in the dielectric medium with the dielectric constant $\epsilon_i (i = m,t,c)$. The interaction between these particles contributes to the total energy of the doped crystal. Although they are close together, the use of the dielectric constant can be justified by the results of recent calculations for the impurity-vacancy interaction in Li_2O.[60] They have demonstrated that for a separation of more than $2a_0$ the association energies of the impurity-vacancy dipole become similar to those obtained from the screened Coulomb interaction in the quasicontinuum model. Let us assume for the sake of simplicity that the impurity-vacancy lattice is periodic with lattice constant a_0^i, where $(a_0^i)^3$ is proportional to the inverse defect concentration and the unit-cell volume of the host crystal. This lattice may be characterized by a Madelung constant $M_i (M_i > 0$ for energetically stable defect arrangements). In the simplest (Coulomb) approximation we can express the defect-defect contribution using the simple formula

$$E_{d\text{-}d}^i = -\frac{M_i q^2}{a_0^i \epsilon_i} .$$

Obviously, the defect-defect interaction energy $E_{d\text{-}d}^i$ depends on the geometrical structure of the host lattice, and therefore can influence the relative values of the DHM in different polymorphs. There are two important factors. First, the lattice constant a_0^i decreases in the sequence $m-t-c$ and thus favors formation of the cubic lattice. Secondly and most importantly, the dielectric constants are different[6] in the m, t, and c phases: $\epsilon_t(38.6) > \epsilon_c(26.9) > \epsilon_m(14.4)$. Therefore this factor also destabilizes the t structure.

Using the experimental unit-cell volumes and the calculated ϵ_i values in the ZrO_2 polymorphs,[6] and assuming a periodic distribution of the NNN dipoles ($x = 0.125$), one can find the $E_{d\text{-}d}^i$ values corresponding to the different phases. The contributions to the DHM values for each phase are equal to $E_{d\text{-}d}^i / x(1-x)$. Then taking the differences we found for $F_0^c - F_0^t$ and $F_0^t - F_0^m$ the values of -0.15 and -0.52 eV respectively. Note that these are comparable with the differences of the DHM values computed by the GULP method (see Table I). Therefore the interactions between defects may play an important role in the mechanism of cubic-phase stabilization. We found that the change of the Madelung con-

TABLE VII. The properties of doped ($x = 0.125$) and pure ZrO_2 crystals computed using the CLUSTER code. E_g is the electronic band gap; $\epsilon_{Ca(Mg)}$ is the one-electron energy of the unoccupied impurity state; q_c and q_d are the total electron populations on cations (including Zr ions and impurities) averaged by the unit cell, and the d populations on the Zr ions, respectively. $q_{Ca(Mg)}$ are the populations of Ca (Mg) ions. Energies are in eV and populations in a.u. Results of the GULP calculations are given in parentheses.

Property	c-ZrO_2	Defect NN Ca-vac.	NNN Ca-vac.	NNN Mg-vac.
a_0 (Å)	4.94 (5.075)	5.00 (5.127)	5.02 (5.120)	4.94 (5.072)
E_g	2.88	3.88	4.00	3.99
$\epsilon_{Ca(Mg)}$		5.8	5.4	5.9
q_c	1.97	1.91	1.92	1.95
q_d	1.51	1.46	1.47	1.51
$q_{Ca(Mg)}$		0.12	0.10	0.11

stant induces a negligible variation of the DHM values (about 0.003 eV for the t-c transition). Thus the difference of the dielectric constants in the two phases makes the most important contribution to the stabilization of the cubic phase. More reliable experimental measurements of the dielectric constants of the high-temperature phases are necessary for better understanding of this effect.

(c) Ionicity. It is well known that directional covalent forces contribute substantially to the Zr-O interaction in ZrO_2. Formation of Zr(d)-O(p) hybrid orbitals and increase of the electronic charge density between the Zr and O atoms are clearly seen from the calculated electronic charge distribution in the ZrO_2 crystals.[29,47] In Table VIII, data from various sources are presented characterizing Zr atomic and Zr(d) orbital populations in the three phases of pure ZrO_2. Despite the different methods used for both the electronic-structure calculation and the charge determination, the general tendency is clear: there is a decrease of ionicity [increase of the Zr and Zr(d) population] for the lower-symmetry phases. The Zr-O overlap population increases as well in the low-symmetry structures.[21,29] These tendencies follow from symmetry considerations,[61,62] which partially forbid mixing of the Zr(d) and O(p) states for t-ZrO_2 and especially for c-ZrO_2. It is also well known that smaller ionicity (higher covalency) favors structures with lower coordination numbers.[63] In fact, the coordination number of Zr decreases from 8 in the fluorite structure to 7 in the m structure through some intermediate value in the t structure. Therefore, the Zr-O covalent bonding is one of the major factors influencing the stability of the low-symmetry structures of ZrO_2.

In contrast, the Ca-O and Mg-O bonds are mostly ionic, thus exhibiting no angular dependence. As discussed in Sec. IV B, the average ionicity of the crystal increases after addition of the divalent impurities. Therefore one can expect that addition of divalent impurities will increase the stability of the high-symmetry phases (especially the cubic phase, which is characteristic of such compounds as CaO and MgO).

(d) Electronic configuration of cations. As one can see from Table VIII, the valence electronic configuration of the Zr ions in c-ZrO_2 is close to the $4d^2$ configuration. In the crystalline field having O_h symmetry this corresponds to the partial occupancy of the t_{2g} levels,[29] resulting in sixfold degeneracy. According to the Jahn-Teller theorem this (cubic) structure around the cation site is unstable, and lattice distortions should appear in order to lower the symmetry and remove the degeneracy. This explains why six different (symmetry-related) tetragonally distorted structures may appear around each Zr atom. The total energy of the crystal is reduced if the local distortion fields around neighboring cations do not disturb each other. Evidently, this corresponds to the formation of the global t structure in which the anion sublattice is displaced along the X_2^- mode (see Fig. 1). The Ca^{2+} or Mg^{2+} dopants have no valence electrons, and the Jahn-Teller distortion does not take place around these ions. This destroys the coherent anionic displacements in the t

TABLE VIII. Electron population analysis (in units of electron charge) on Zr atoms in the three ZrO_2 polymorphs. "Zr" is the total population and "Zr d" is the population on the d orbitals of the Zr atoms.

Method	Population analysis	Geometry		m	t	c
Hartree-Fock	Mulliken	optimized	Zr	0.750[a]	0.715[b]	0.679[b]
pseudopotential[c]			Zr d	1.302[a]	1.246[b]	1.162[b]
FLAPW[d]	charge-density integration	experimental	Zr d		1.69	1.42
LDA LCAO[e]	Mulliken	experimental	Zr	2.09	2.05	1.91
			Zr d	1.91	1.94	1.73
Cluster DV-X_α[f]	Mulliken	experimental	Zr		1.1	0.9
CNDO[g]	Löwdin	experimental	Zr	0.9	1.0	1.0
		This work				
Hartree-Fock	Mulliken	optimized	Zr	1.065	0.984	0.962
Pseudopotential[h]			Zr d	0.868	0.807	0.792
INDO	Löwdin	optimized	Zr	2.36	2.01	1.97
			Zr d	1.88	1.53	1.51

[a]Reference 21.
[b]Reference 29.
[c]Hay and Wadt large-core ECP (Ref. 19) on Zr atoms. In this method the total electron population on Zr atoms is smaller than that on Zr d functions. This is an artifact of the basis set used, as discussed in Ref. 29.
[d]Reference 47.
[e]Reference 31. LDA is the local-density approximation.
[f]Reference 61.
[g]Reference 62. CNDO is the complete neglect of differential overlap.
[h]Hay and Wadt small-core ECP (Ref. 19) on Zr atoms.

structure and reduces the energy separation between the t and c phases in the doped crystals.

The discussion above shows that the stabilization of cubic zirconia by impurities is a complex phenomenon comprising significant changes of both atomic and electronic structures of the doped crystals. In our model calculations we have identified some of the basic factors controlling the relative stability of the t- and c-ZrO_2 polymorphs and discussed them in the context of aligned dipoles. However, in order to understand this effect in full, more sophisticated models of the solid solution should be employed which take into account also the distribution, mobility, and clustering of defects,[6,50] their vibrational and configurational entropy,[41] the nonlocal compensation of the charge of the impurity (for instance, due to segregation of the charged defects to the grain boundaries[64]), and the reorientation of dipoles. Moreover, these results for different models should be properly averaged according to their statistical weight and temperature (for instance, by means of the Monte Carlo technique). Solution of these challenging problems will provide a better understanding of the mechanisms of phase transitions and promote the technological implementation of zirconia-based ceramics.

ACKNOWLEDGMENTS

Financial support from the Royal Society (London), The Royal Institution, UK AEA Technology, Harwell, and the University of Torino is gratefully acknowledged. The authors thank Dr. A. H. Harker for stimulating discussions and Dr. J. Gale for performing Hartree-Fock calculations of the ZrO_2 molecule, for his permission to use the GULP code, and for valuable comments. The *ab initio* Hartree-Fock calculations of the three ZrO_2 polymorphs were performed in close collaboration with the Theoretical Chemistry Group in the Department of Inorganic, Physical, and Materials Science in the University of Torino. E.V.S. is grateful to R. Orlando, C. Pisani, C. Roetti, and E. Ruiz for their help, fruitful discussions, and permission to use the CRYSTAL code.

[1]E. Ryshkewitch and D. W. Richerson, *Oxide Ceramics. Physical Chemistry and Technology* (General Ceramics, Haskell, NJ, 1985).
[2]C. J. Howard, R. J. Hill, and B. E. Reichert, Acta Crystallogr. Sect. B **44**, 116 (1988).
[3]R. N. Patil and E. C. Subbarao, J. Appl. Crystallogr. **2**, 281 (1969).
[4]P. Aldebert and J.-P. Traverse, J. Am. Ceram. Soc. **68**, 34 (1985).
[5]K. Negita, Acta Metall. **37**, 313 (1989).
[6]A. Dwivedi and A. N. Cormack, Philos. Mag. **61**, 1 (1990).
[7]A. N. Cormack and S. C. Parker, J. Am. Ceram. Soc. **73**, 3220 (1990).
[8]C. Pisani, R. Dovesi, and C. Roetti, *Hartree-Fock Ab Initio Treatment of Crystalline Solids,* Lecture Notes in Chemistry Vol. 48 (Springer, Berlin, 1988).
[9]R. Dovesi, V. R. Saunders, and C. Roetti, *CRYSTAL 92, User's Manual* (Universita' di Torino and SERC Daresbury Lab., 1992).
[10]General Utility Lattice Program, Julian Gale, Imperial College, London, U.K. (1993).
[11]A. L. Shluger and E. A. Kotomin, Phys. Status Solidi B **108**, 673 (1981); A. L. Shluger, Theor. Chim. Acta **66**, 355 (1985).
[12]E. Stefanovich, E. Shidlovskaya, A. Shluger, and M. Zakharov, Phys. Status Solidi B **160**, 529 (1990).
[13]H. L. Lukas, J. Weiss, and E.-Th. Henig, CALPHAD: Computer Coupling of Phase Diagrams and Thermochemistry **3**, 229 (1982).
[14]Y. Du, Z. Jin, and P. Huang, J. Am. Ceram. Soc. **75**, 3040 (1992).
[15]Y. Du and Z. Jin, CALPHAD **15**, 59 (1991).
[16]I. Prigogine, *The Molecular Theory of Solutions* (North-Holland, Amsterdam, 1957); E. A. Gugenheim, *Mixtures* (Clarendon, Oxford, 1952).
[17]CRC Handbook of Chemistry and Physics, 65th ed., edited by R. C. Weast (Chemical Rubber, Boca Raton, 1985).
[18]R. J. Ackermann, E. G. Rauh, and C. A. Alexander, High Temp. Sci. 7, 304 (1975).
[19]P. J. Hay and W. R. Wadt, J. Chem. Phys. **82**, 299 (1985).
[20]P. H. Durand and J. C. Barthelat, Theor. Chim. Acta **38**, 283 (1975).
[21]R. Orlando, D. Pisani, C. Roetti, E. Ruiz, and E. Stefanovich (unpublished).
[22]R. A. Evarestov, *Quantum-Chemical Methods of Solid State Theory* (Leningrad State University, Leningrad, 1982).
[23]J. A. Pople and D. L. Beveridge, *Approximate Molecular Orbital Theory* (McGraw-Hill, New York, 1970).
[24]S. N. Mysovsky (private communication).
[25]S. R. Langhoff and C. W. Bauschlicher, Jr., J. Chem. Phys. **89**, 2160 (1988).
[26]CADPAC5 developed by R. D. Amos *et al.*, Cambridge U.K. (1992).
[27]Y. Sakai, E. Miyoshi, M. Klobukowski, and S. Huzinaga, J. Comput. Chem. **8**, 256 (1987).
[28]A. D. McLean and G. S. Chandler, J. Chem. Phys. **72**, 5639 (1980).
[29]R. Orlando, C. Pisani, C. Roetti, and E. Stefanovich, Phys. Rev. B **45**, 592 (1992).
[30]C. R. Aita and C.-K. Kwok, J. Am. Ceram. Soc. **73**, 3209 (1990).
[31]F. Zandiehnadem and R. A. Murray, Physica B **150**, 19 (1988).
[32]R. Pandey, J. E. Jaffe, and A. B. Kunz, Phys. Rev. B **43**, 9228 (1991).
[33]R. C. Whited, C. J. Flaten, and W. C. Walker, Solid State Commun. **13**, 1903 (1973).
[34]M. L. Bortz, R. G. French, D. J. Jones, R. W. Kasowski, and F. S. Ohuchi, Phys. Scr. **41**, 537 (1990).
[35]H. J. F. Jansen, Phys. Rev. B **43**, 7267 (1991).
[36]S. T. Pantelides, D. J. Mickish and A. B. Kunz, Phys. Rev. B **10**, 5203 (1974).
[37]R. A. Evarestov, E. A. Kotomin, and A. N. Ermoshkin, *Molekularniye Modeli Tochechnikh Defektov v Shirokoschelevikh Tverdikh Telakh* (Izd. Zinatne, Riga, 1983) (in Russian).
[38]This technique has been reviewed in J. Chem. Soc. Faraday Trans. 2 **85**, (1989), special issue, edited by C. R. A. Catlow

and A. M. Stoneham.
[39]G. V. Lewis and C. R. A. Catlow, J. Phys. C **18**, 1149 (1985).
[40]M. Hillert and T. Sakuma, Acta Metall. Mater. **39**, 1111 (1991).
[41]R. C. Garvie and S.-K. Chan, Physica B **150**, 203 (1988); S.-K. Chan, *ibid.* **150**, 212 (1988).
[42]J. R. Morris and R. J. Gooding, Phys. Rev. B **46**, 8733 (1992).
[43]Th. Proffen, R. B. Neder, F. Frey, and W. Assmus, Acta Crystallogr. Sect. B **49**, 599 (1993).
[44]R. B. Neder, F. Frey, and H. Schulz, Acta Crystallogr. Sect. A **46**, 799 (1990).
[45]U. Martin, H. Boysen, and F. Frey, Acta Crystallogr. Sect. B **49**, 403 (1993).
[46]H. J. Rossell, J. R. Sellar, and I. J. Wilson, Acta Crystallogr. Sect. B **47**, 862 (1991).
[47]H. J. F. Jansen and J. A. Gardner, Physica B **150**, 10 (1988).
[48]Y. Zhou and H. J. F. Jansen, Bull. Am. Phys. Soc. **38**, 674 (1993).
[49]M. Leslie (unpublished).
[50]W. C. Mackrodt and P. M. Woodrow, J. Am. Ceram. Soc. **69**, 277 (1986).
[51]V. Butler, C. R. A. Catlow, and B. E. F. Fender, Radiat. Eff. **73**, 273 (1983); V. Butler, C. R. A. Catlow, and B. E. F. Fender, Solid State Ionics **5**, 539 (1981).
[52]M. Morinaga, J. B. Cohen, and J. Faber, Jr., Acta Crystallogr. **36**, 520 (1980).
[53]M. Yashima, N. Ishizawa, and M. Yoshimura, J. Am. Ceram. Soc. **75**, 1541 (1992).
[54]L. M. Moroney, in *Nonstoichiometric Compounds*, Vol. 23 of Advances in Ceramics, edited by C. R. A. Catlow and W. C. Mackrodt (American Ceramic Society, Westerville, 1986).
[55]A. B. Sobolev, A. N. Varaksin, O. A. Keda, and A. P. Khaimenov, Fiz. Tverd. Tela (Leningrad) **32**, 2255 (1990) [Sov. Phys. Solid State **32**, 1310 (1990).
[56]D. E. Ellis, J. Guo, and D. J. Lam, J. Am. Ceram. Soc. **73**, 3231 (1990); D. E. Ellis and D. J. Lam, Physica B **150**, 25 (1988).
[57]S. M. Sim and V. S. Stubican, J. Am. Ceram. Soc. **70**, 521 (1987).
[58]P. Duran, P. Recio, and J. M. Rodriguez, J. Mater. Sci. **22**, 4348 (1987).
[59]M. Hillert, J. Am. Ceram. Soc. **74**, 2005 (1991).
[60]J. L. Gavartin, A. L. Shluger, and C. R. A. Catlow, J. Phys. Condens. Matter **5**, 7397 (1993).
[61]M. Morinaga, H. Adachi, and M. Tsukada, J. Phys. Chem. Solids **44**, 301 (1983).
[62]R. A. Evarestov, A. V. Leko, and A. R. Sokolov, Dokl. Akad. Nauk SSSR **299**, 1185 (1988).
[63]J. A. Van Vechten, Phys. Rev. **187**, 1007 (1969); J. C. Phillips, Phys. Today **23 (2)**, 23 (1970); A. Garcia and M. L. Cohen, Phys. Rev. B **47**, 4215 (1993); **47**, 4221 (1993).
[64]S.-L. Hwang and I. W. Chen. J. Am. Ceram. Soc. **73**, 3269 (1990).

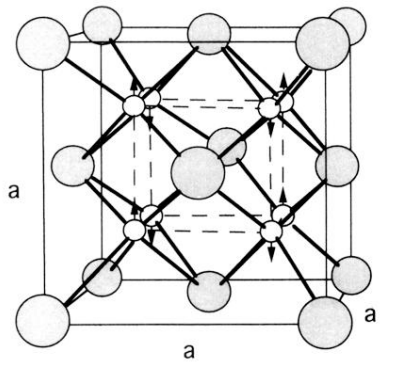

a

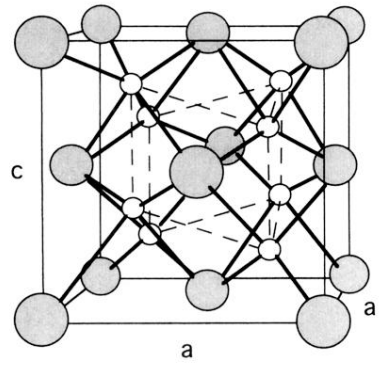

b

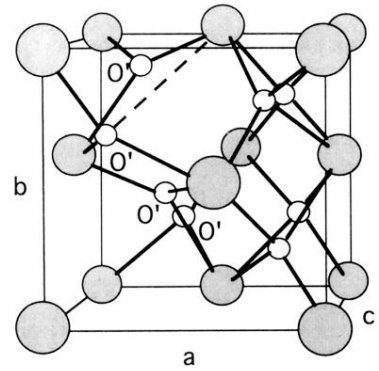

c

FIG. 1. Schematics of the three ZrO_2 polymorph structures. Small circles represent the oxygen atoms; large shaded circles represent the zirconium atoms. a, b, and c indicate the crystalline axes. (a) c-ZrO_2. The arrows show the directions of displacements of the oxygen atoms corresponding to the X_2^- distortion which transforms the c structure into the t structure. (b) t-ZrO_2. Note the deformation of the oxygen sublattice (dashed lines) with respect to that in the c structure. (c) m-ZrO_2. In contrast to the t and c structures Zr atoms are seven coordinated and O′ atoms are three coordinated: the Zr-O′ bond which is shown by a dashed line is broken. Note that the unit cell is rotated with respect to that in (b).

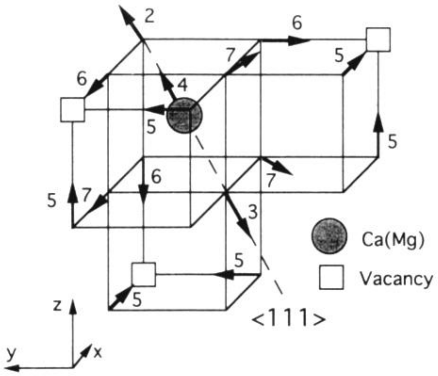

FIG. 3. Schematic of the NNN Ca (Mg) -vacancy dipole in c-ZrO_2. There are no separate dipoles in the lattice. Each impurity cation is surrounded by three oxygen vacancies symmetrically with respect to the threefold $\langle 111 \rangle$ axis. Arrows show the directions of ionic displacements obtained in the GULP calculations. The numbers by the arrows correspond to the relaxation modes in Table VI.